NMR Studies of the Interaction of a Type II Dihydrofolate Reductase with Pyridine Nucleotides Reveal Unexpected Phosphatase and Reductase Activity†

Wayne H. Pitcher, III,‡ Eugene F. DeRose,‡ Geoffrey A. Mueller,‡ Elizabeth E. Howell,§ and Robert E. London*,‡

Laboratory of Structural Biology, MR-01, National Institute of Environmental Health Sciences, National Institutes of Health, Box 12233, Research Triangle Park, North Carolina 27709, and Biochemistry, Cell, and Molecular Biology Department, F327B Walters Life Sciences, University of Tennessee, Knoxville, Tennessee 37996

Received June 9, 2003; Revised Manuscript Received July 29, 2003

ABSTRACT: The interaction of type II R67 dihydrofolate reductase (DHFR) with its cofactor nicotinamide adenine dinucleotide phosphate ($NADP^+$) has been studied using nuclear magnetic resonance (NMR). Doubly labeled [U-^{13}C,^{15}N]DHFR was obtained from *Escherichia coli* grown on a medium containing [U-^{13}C]-D-glucose and $^{15}NH_4Cl$, and the 16 disordered N-terminal amino acids were removed by treatment with chymotrypsin. Backbone and side chain NMR assignments were made using triple-resonance experiments. The degeneracy of the amide ^1H and ^{15}N shifts of the tetrameric DHFR was preserved upon addition of $NADP^+$, consistent with kinetic averaging among equivalent binding sites. Analysis of the more titration-sensitive DHFR amide resonances as a function of added $NADP^+$ gave a K_D of 131 ± 50 μM, consistent with previous determinations using other methodology. We have found that the ^1H spectrum of $NADP^+$ in the presence of the R67 DHFR changes as a function of time. Comparison with standard samples and mass spectrometric analysis indicates a slow conversion of $NADP^+$ to NAD^+, i.e., an apparent $NADP^+$ phosphatase activity. Studies of this activity in the presence of folate and a folate analogue support the conclusion that this activity results from an interaction with the DHFR rather than a contaminating phosphatase. ^1H NMR studies of a mixture of $NADP^+$ and NADPH in the presence of the enzyme reveal that a ternary complex forms in which the N-4A and N-4B nuclei of the NADPH are in the proximity of the N-4 and N-5 nuclei of $NADP^+$. Studies using the $NADP^+$ analogue acetylpyridine adenosine dinucleotide phosphate ($APADP^+$) demonstrated a low level of enzyme-catalyzed hydride transfer from NADPH. Analysis of DHFR backbone dynamics revealed little change upon binding of $NADP^+$. These additional catalytic activities and dynamic behavior are in marked contrast to those of type I DHFR.

Dihydrofolate reductase (DHFR)[1] catalyzes the NADPH-dependent reduction of dihydrofolate to tetrahydrofolate, an essential factor for one-carbon metabolism. Chromosomal bacterial DHFR is the target of antifolate drugs such as trimethoprim, a broad-spectrum antibiotic used in both human and veterinary medicine (*1*, *2*). In bacteria, resistance to trimethoprim can be conferred by a plasmid encoding DHFRs with reduced trimethoprim affinity (*3*). While most of these plasmid-encoded DHFRs have primary sequences related to chromosomal DHFR, type II DHFRs are evolutionarily unrelated to other DHFRs and are insensitive to trimethoprim (*4*−*6*).

Type II R67 DHFR is a homotetramer (34 kDa total) with 78-amino acid subunits. The crystal structure of a truncated form of the protein, which lacked the 16 disordered N-terminal residues, has been determined previously (*7*). The structure is characterized by a central pore traversing the protein and containing the active site(s). The subunits of the tetramer are related by 222 symmetry. Isothermal titration calorimetry studies have shown that, in addition to the catalytically active ternary complex and its analogues, R67 DHFR can form ternary complexes involving pairs of NADPH or folate molecules (*8*). Structural information about the DHFR−cofactor, DHFR−substrate, and ternary complexes is limited, in part due to the combination of symmetry and binding stoichiometry of DHFR. Less than full occupancy of ligand binding sites results in electron density with partial occupancy and leads to difficulty in interpreting diffraction data.

Transferred NOE experiments (*9*) and interligand NOE experiments (*10*) have been used to obtain information about the conformation of bound $NADP^+$ and about the arrangement of the ternary folate−$NADP^+$−DHFR complex. These studies have demonstrated that bound $NADP^+$ is characterized by a *syn* conformation about the ribonicotinamide bond and an *anti* conformation of the glycosidic bond of adenosine. In the ternary $NADP^+$−folate−DHFR complex, strong interligand NOEs were observed between the nicotinamide H-4 and H-5 protons and the H-9 protons of the folate. Studies of ternary complexes employing folate analogues

† This research was supported by NSF Grant MCB-0131394 (to E.E.H.).

* To whom correspondence should be addressed. Phone: (919) 541-4879. Fax: (919) 541-5707. E-mail: london@niehs.nih.gov.

‡ National Institutes of Health.

§ University of Tennessee.

[1] Abbreviations: $APADP^+$, 3-acetylpyridine adenine dinucleotide phosphate; APADPH, reduced 3-acetylpyridine adenine dinucleotide phosphate; CSI, chemical shift index; DMDDF, 2-desamino-2-methyl-5,8-dideazafolate; DHFR, dihydrofolate reductase; EXSY, exchange spectroscopy; ILOE, interligand Overhauser effect; ITC, isothermal titration calorimetry; NOE, nuclear Overhauser effect.

10.1021/bi0349874 CCC: $25.00
Published on Web 09/03/2003

provided further support for a complex in which the substrate and cofactor are arrayed with the nicotinamide and pterin groups near each other at the center of the pore, with the AMP moiety of $NADP^+$ and the glutamate group of folate extending in opposite directions toward the lip on either side of the pore. The relative orientation of the nicotinamide and pterin ring systems was found to be fairly similar to the recently determined orientation in pteridine reductase [PDB entry 1E92 (*11*)], involving partial stacking of the nicotinamide and pterin ring systems in an *endo* geometry. In that system, the ribonicotinamide geometry in the ternary $NADP^+$−pteridine−reductase system is also *syn*; however, since the latter catalyzes a B-side hydride transfer in contrast with the A-side transfer of R67 DHFR, it would be necessary to place the pteridine ring on the opposite side of the nicotinamide ring.

In the study presented here, we have found that R67 DHFR apparently catalyzes the slow dephosphorylation of $NADP^+$ to yield NAD^+. Among other conclusions, this result provides an alternate explanation for the spectral changes previously observed in the related R388 type II DHFR (*12*). We have also prepared [U-^{13}C,^{15}N]R67 DHFR to assign the resonances of the protein. Changes in amide chemical shifts in HSQC (heteronuclear single-quantum coherence) spectra upon titration of DHFR with $NADP^+$ (or folate) provide further insight into the orientation of the bound cofactor. Analysis of backbone dynamics provides a clearer picture of the motions of the protein. Finally, we have obtained interligand Overhauser effect data for the ternary $NADP^+$−NADPH−DHFR complex that demonstrate the proximity of the N-4 protons in the reduced and oxidized species.

MATERIALS AND METHODS

Doubly labeled recombinant His tag-labeled [U-^{13}C,^{15}N]-R67 DHFR was obtained from *Escherichia coli* grown on a minimal medium containing [U-^{13}C]-D-glucose and $^{15}NH_4$-Cl. The His-tagged DHFR was purified using a Ni−NTA resin (*13*). The His tag sequence as well as the 16 natural N-terminal amino acids on each subunit were removed by chymotrypsin treatment, yielding a fully active protein (*7*). Enzyme purification and chymotrypsin cleavage were monitored by activity measurements using a Perkin-Elmer lambda3a spectrophotometer interfaced with an IBM PS2 personal computer as previously described (*13*). Briefly, assays were performed at 30 °C in 10 mM Tris, 1 mM EDTA, pH 7 buffer. DHFR reduction of DHF and NADPH was monitored at 340 nm. $NADP^+$, folic acid, and acetylpyridine adenine dinucleotide phosphate ($APADP^+$) were obtained from Sigma (St. Louis, MO) and used without further purification. A standard sample of reduced APADP (APADPH) was prepared by reduction of 1 mM $APADP^+$ by 10 mM $NaCNBH_3$ in 25 mM phosphate buffer (pH 7.0).

Lyophilized DHFR was dissolved in 25 mM sodium phosphate buffer (pH 7.0) and a 95% H_2O/5% D_2O mixture for use in NMR experiments. The total tetramer concentration was 0.7 mM (2.8 mM monomer). NMR experiments were performed on a Varian UNITY plus 500 NMR spectrometer at 25 °C using a Nalorac 5 mm triple-resonance probe. Standard Varian ProteinPack experiments were carried out. To obtain assignments, the following experiments were performed: two-dimensional (2D) ^{1}H−^{15}N HSQC, 2D ^{1}H−^{13}C CT-HSQC, three-dimensional (3D) HNCACB, 3D CB-CA(CO)NH, 3D ^{15}N-edited TOCSY-HSQC, 3D C(CO)NH, and 3D H(CCO)NH (*14*−*16*). Backbone ^{15}N relaxation experiments were carried out by selecting the T_1 and T_2 options in Varian's gNhsqc ^{1}H−^{15}N HSQC pulse sequence. Heteronuclear ^{1}H−^{15}N NOE measurements were made using the sequence of Farrow et al. (*17*). Relaxation experiments were performed on a Varian UNITY plus 500 NMR spectrometer (DHFR alone) or a Varian UNITY INOVA 600 NMR spectrometer (DHFR with $NADP^+$). Data were processed with NMRPipe (*18*) and analyzed with NMRView (*19*). The relaxation analysis module of NMRView 5.0.4 was corrected to properly output errors as posted on our website (http://dir.niehs.nih.gov/dirnmr/nmrview.htm). Errors reported here are standard errors as given by the relaxation analysis module. Concentrated solutions of $NADP^+$ and folate were prepared in the NMR buffer. Aliquots of these solutions were added to achieve the desired $NADP^+$:DHFR or folate:DHFR ratio. $NADP^+$ and folate titrations were also observed with the ^{1}H−^{15}N HSQC experiment on a Varian UNITY plus 500 NMR spectrometer. In titration experiments, total amide shifts were calculated as the total distance the peak moved, weighting the change in the ^{1}H chemical shift by a factor of 5. Thus, the weighted shift $= [(5\Delta\delta_{^1H})^2 + \Delta\delta_{^{15}N}{}^2]^{1/2}$. K_D values based on titration experiments were calculated according to the method of Connors (*20*).

Protein backbone dynamics were analyzed using programs obtained from A. Palmer (available free via the Internet at http://cpmpnet.columbia.edu/dept/gsas/biochem/labs/palmer/software/diffusion.html). The program pdbinertia (version 1.11) was used to estimate the principal moments of inertia and the principal axes of inertia for DHFR, and the program quadric (version 1.12) was used to determine the validity of different diffusion models (*21*, *22*). The tetramer crystal structure (PDB entry 1VIE) was used for these calculations. The program Modelfree (version 4.01) was used to fit various dynamical models and parameters for backbone ^{15}N spins (*23*). The values for τ_m, D_{ratio}, θ, and ϕ obtained from the axially symmetric model fit from quadric were used as input values for Modelfree.

The Modelfree approach selects from among five dynamic descriptions for the nucleus in question, corresponding to (1) the generalized order parameter (S^2) only, (2) S^2 and τ_e (the correlation time for internal motions), (3) S^2 and R_{ex} (a term used to describe the contributions of microsecond to millisecond time scale motions to T_2), (4) model 2 with R_{ex}, and (5) two components of internal motion characterized by $\tau_f < \tau_s < \tau_c$. Model selection was based on Akaike's Information Criteria (AIC) (*24*). Errors in S^2 reported here are standard errors as given by Modelfree.

Degradation of $NADP^+$ to NAD^+ was observed by ^{1}H NMR at 500 MHz on a Varian UNITY INOVA 500 NMR spectrometer at 25 °C. The following spectral parameters were used: spectral width of 6500 Hz, acquisition time of 1.025 s, 6656 complex points, recycle delay of 1 s, and 2048 transients collected. Spectra were collected approximately every 70 min. Samples consisted of 0.5 mM DHFR and 5 mM $NADP^+$ in 25 mM sodium phosphate in D_2O (pD 7.0). For some kinetic experiments, folate (final concentration of 25 mM) or the folate analogue DMDDF (2-deamino-2-methyl-5,8-dideazafolate, final concentration of 10 mM) was added (*10*). Limited ^{31}P NMR data for this reaction were

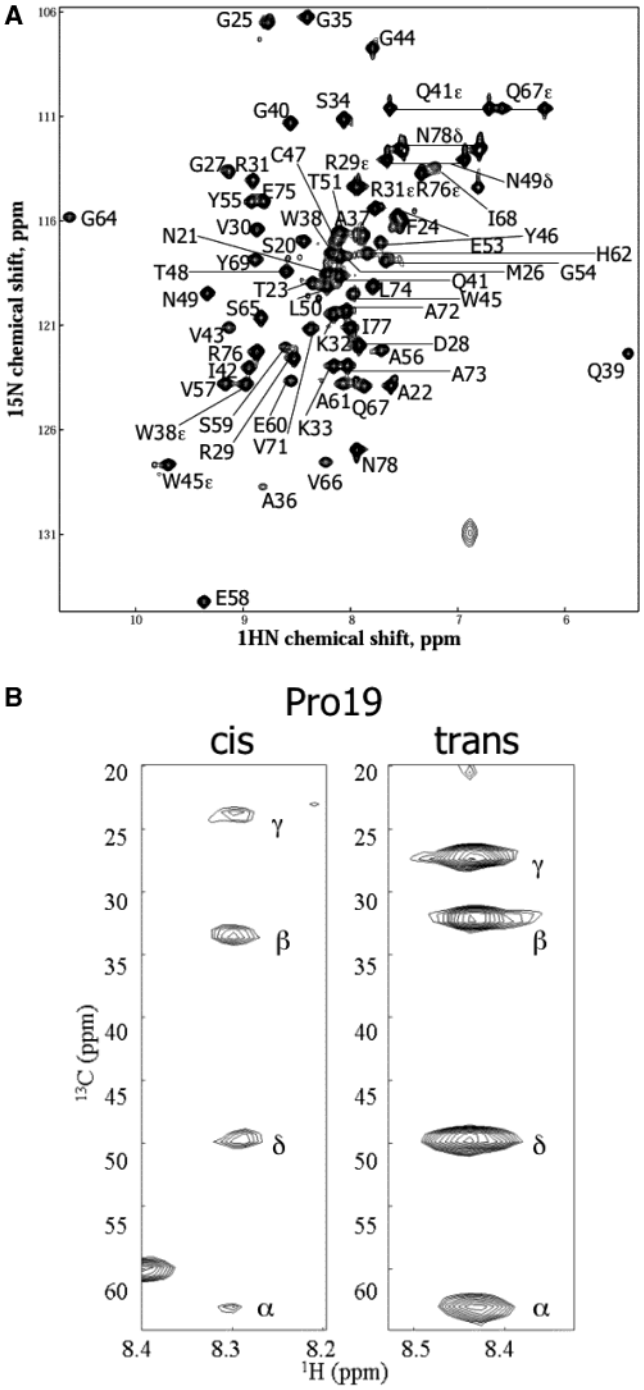

FIGURE 1: (A) Assigned ^{15}N HSQC spectrum of R67 DHFR (62-amino acid protein). (B) F_1 strips of the (H)C(CO)NH TOCSY spectrum at the ^{15}N and ^{1}H chemical shifts of *cis* Ser20 and *trans* Ser20 are shown.

also obtained on a Varian Gemini 300 instrument, operating at a resonance frequency of 121.5 MHz. Kinetic data were fit with Kaleidagraph (Synergy Software, Reading, PA). Chemical shift titration data were analyzed using the nonlinear least-squares capability of Mathematica (Wolfram Research, Champaign, IL).

RESULTS

Assignment of NMR Spectra. The assigned $^{1}H-^{15}N$ HSQC spectrum of [U-^{13}C,^{15}N]R67 DHFR is shown in Figure 1A. As discussed in Materials and Methods, the labeled enzyme was treated with chymotrypsin to remove the 16 disordered N-terminal residues, following the procedure previously used in the crystal structure studies (*7*). Assignment of the backbone ^{1}H, ^{15}N, $^{13}C^{\alpha}$, and $^{13}C^{\beta}$ resonances was complete except for the four prolines (residues 19, 52, 63, and 70 in the full protein sequence), for which only $^{13}C^{\alpha}$ and $^{13}C^{\beta}$ are assigned, and the N-terminal residues (Val17 and Phe18), which are unassigned. Side chain assignments were mostly complete, with ~89% of ^{1}H, ~69% of ^{13}C (aromatics and carbonyls were not assigned), and ~73% of ^{15}N resonances assigned. The assignment of Q67ϵ protons in the $^{1}H-^{15}N$ HSQC spectrum is tentative. We base our assignment of Q67ϵ on the large chemical shift change observed upon binding $NADP^{+}$ and the disappearance due to broadening of the peaks upon binding of folate. In general, CSI analysis of the $^{1}H^{\alpha}$, ^{15}N, $^{13}C^{\alpha}$, and $^{13}C^{\beta}$ shifts was consistent with the secondary structure observed in the crystal (data not shown) (*25*). Additional resonances arising from residues in the N-terminal region of the protein were observed. This region of the protein contains a proline at position 3 (Pro19 using the numbering for the complete peptide sequence), introducing the possibility that the additional resonances could arise from *cis*−*trans* isomerism of the Phe18−Pro19 bond. For the *cis*-proline isomer, alternate $^{13}C^{\alpha}$ and $^{13}C^{\beta}$ chemical shifts were observed for Pro19, Ser20, and Asn21, and alternate backbone ^{1}H and ^{15}N chemical shifts were observed for Ser20, Asn21, and Ala22. Figure 1B compares the observed resonances for the *cis* and *trans* isomers of Pro19. The significant upfield shift of the Pro19 C-γ resonance is characteristic of *cis* X−Pro bonds (*26*). Further, a higher *cis*:*trans* ratio (approximately 1:3 for R67 DHFR) is typical of peptides containing an aromatic residue immediately preceding proline (*27*). We also note that *cis*-proline has been observed previously in unfolded R67 DHFR (*28*). The ^{1}H, ^{15}N, and ^{13}C chemical shifts have been deposited in the BioMagResBank (http://www.bmrb.wisc.edu) under BMRB accession number 5237.

Cofactor Binding. In general, the analysis of the interaction of type II DHFR with ligands is complex since ligand binding will break the symmetry that characterizes the unliganded tetramer. However, kinetic averaging of the ligand between symmetry-related positions can theoretically remove some or all of this inequivalence on the NMR time scale. It was hypothesized that $NADP^{+}$ might be a good choice in this regard because of its relatively weak binding and tendency to form a 1:1 complex with the enzyme (*8*). Titration of R67 DHFR with $NADP^{+}$ at 25 °C resulted in progressive shifts of the amide proton and nitrogen resonances, with varying degrees of broadening. In no case were separate resonances observed which would arise from inequivalence of the corresponding residues in the different peptide chains. Titration curves for several of the more significantly shifted residues are shown in Figure 2. Analysis of the data for the most strongly shifted ^{15}N resonances **(**Lys32, Lys33, Gly35, Ser59, Ser65, Val71, Ala73, and Leu74 using standard relations (e.g., ref *20*)) gave a K_D of 132 ± 51 μM. Similarly, analysis of the most strongly shifted ^{1}H data **(**Lys33, Gly35, Glu39, Glu60, Ala61, Gly64, Ala72, Ala73, and Leu74**)** gave a K_D of 130 ± 53 μM. These values are slightly greater than the value of 99 μM previously reported by Bradrick et al. (*8*), most probably due to competitive binding by the phosphate buffer, although the difference is within the experimental error.

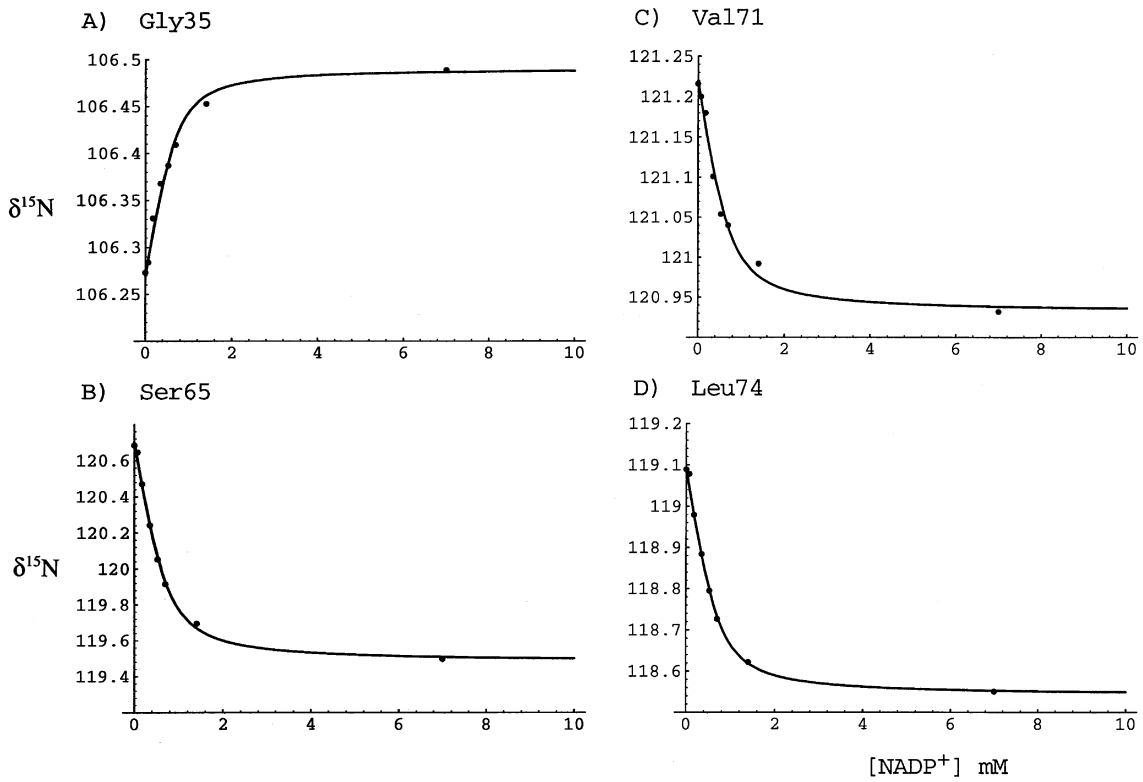

FIGURE 2: ^{15}N chemical shifts for (A) Gly35, (B) Ser65, (C) Val71, and (D) Leu74 as a function of NADP$^+$ concentration. The sample contained 0.7 mM DHFR (tetramer) in 25 mM phosphate (pH 7.0). Spectra were obtained at 25 °C. Curves correspond to computed fits determined as described in the text.

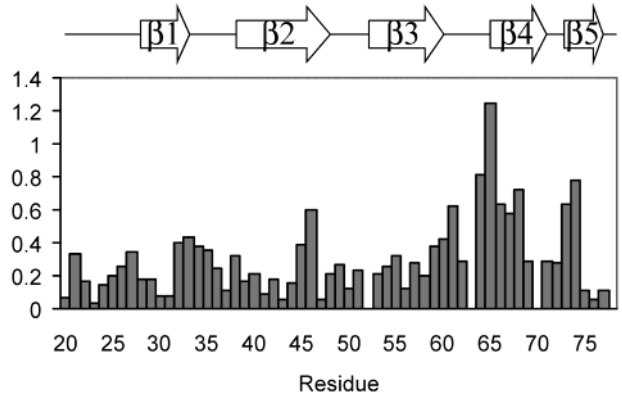

FIGURE 3: Amide chemical shift perturbations resulting from the addition of 7 mM NADP$^+$ to a sample initially containing 0.7 mM R67 DHFR. The weighted shift $= [(5\Delta\delta_{^1H})^2 + \Delta\delta_{^{15}N}{}^2]^{1/2}$. Solutions were in 25 mM phosphate (pH 7.0) and spectra obtained at 25 °C.

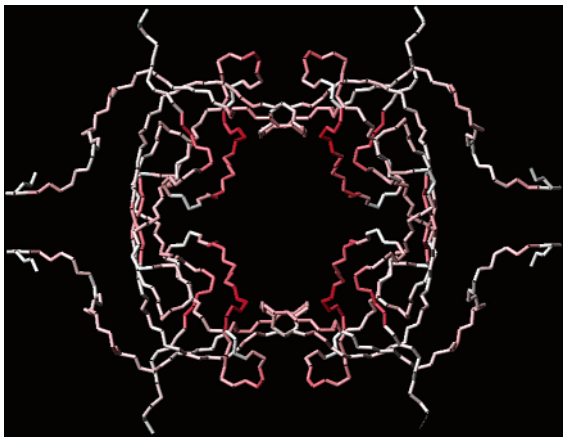

FIGURE 4: α-Carbon backbone of R67 DHFR, with the residues colored by chemical shift change upon binding of NADP. A more intense red indicates a greater chemical shift change. Shown is a view of DHFR looking along the axis of the central pore. The following residues have atoms in the pore, as determined by CAST (*41*): Lys32, Lys33 (C^β only), Ser34, Gly35, Ala36 (N only), Tyr46, Thr48 ($O^{\gamma 1}$ only), Leu50, Thr51, Gly64, Ser65, Val66, Gln67, Ile68, Tyr69, Pro70, and Ala73. This figure was produced with MOLMOL.

The distribution of amide chemical shifts resulting from NADP$^+$ binding is summarized in Figure 3. In general, the residues exhibiting the largest amide shifts were those that line the pore (*7*, *29*), as is apparent from the color-coded model shown in Figure 4. Amide groups in the vicinity of Lys32 also exhibited significant shift perturbations, presumably related to the proximity of this residue to the phosphate groups on the NADP$^+$ cofactor. In addition to residues on β-strand 4 lining the pore, the residues on β3 also shifted significantly upon binding of NADP$^+$. The shifts observed for the β3 amide groups could result from a combination of the proximity to the bound aromatic and charged groups on the ligands and altered interactions with β4 due to repositioning of this strand as it binds to the cofactor. Interestingly, the amide resonances for Tyr55, Val57, and Ser59 which hydrogen bond with residues on β4 exhibit larger shift perturbations than residues Ala56 and Glu58 which do not hydrogen bond with residues in β4. As is apparent from Figure 3, several other residues that are not positioned in the pore and would not be anticipated to make contact with the NADP(H) cofactor also exhibit significant amide shifts. In nearly all of these cases, the residues are located in the β-sheet structure of the enzyme. It seems probable that a

structural adjustment to $NADP^+$ binding which perturbs the β-sheet structure will alter the hydrogen bonding interactions of these residues, perhaps explaining the observed chemical shift changes.

Attempts to directly observe NOE interactions between the protons of $NADP^+$ and DHFR have proven to be uniformly unsuccessful (data not shown[2]). This may arise from several factors, the most significant limitation resulting from the tetrameric structure of the enzyme. For any given binding mode, the various $NADP^+$ protons would be positioned near only one of the four equivalent residues on the tetramer. Since fast exchange conditions prevail, this would have the effect of reducing the level of the observed interaction by 75%. A second limitation arises from the likelihood that the folate/dihydrofolate substrate provides an important component of the NADP(H) binding site; as a result, the position of the latter is more poorly defined in the absence of substrate. Isothermal titration calorimetry studies have demonstrated that the binding of the substrate and the binding of the cofactor are highly cooperative (*8*). Recent interligand Overhauser effect studies performed on the folate−$NADP^+$−DHFR complex indicate that the pteridine and nicotinamide ring systems may be at least partially stacked in the active site (*10*). Thus, the position of NADP(H) would be more tightly constrained in the presence of the folate/dihydrofolate substrate. Such a structure would be similar to the transition state geometry calculated by Andres et al. (*32*). Consequently, the interactions of the $NADP^+$ with the enzyme in the absence of the folate/dihydrofolate substrate are weaker and more variable, and hence less likely to produce strong NOEs. Although we also have obtained NMR data for the ternary folate−$NADP^+$−DHFR complex, the tighter binding and slower exchange kinetics in this complex lift the degeneracy of many of the resonances, making the enzyme NMR spectra considerably more complex (data not shown).

Catalytic Degradation of $NADP^+$ to NAD^+. Proton NMR studies of samples containing $NADP^+$ in the presence of R67 DHFR revealed unanticipated, time-dependent changes that were most readily apparent in the sparse downfield region of the spectrum containing the nicotinamide N-2 and N-6 resonances. In particular, we observed the gradual appearance of two resonances positioned 0.06 and 0.08 ppm downfield of the NH2 and NH6 peaks of $NADP^+$. The two additional resonances were significantly narrower than the corresponding NH2 and NH6 resonances of $NADP^+$. The intensity of these resonances continued to increase over a period of hours to days, depending on the enzyme concentration. Comparison of the resonances with a number of standard samples, including nicotinamide mononucleotide, nicotinamide riboside, and NAD^+, revealed that the new resonances corresponded to NAD^+. Further confirmation of this result was obtained from mass spectrometric analysis and ^{31}P NMR studies, which showed the progressive formation of inorganic phosphate in a sample initially containing only $NADP^+$ and R67 DHFR (data not shown).

The catalytic dephosphorylation of $NADP^+$ to yield NAD^+ can in principle result from either a $NADP^+$ phosphatase contaminant or a side reaction catalyzed by R67 DHFR. Mitochondrial $NADP^+$ phosphatases have been identified in several plants and other species (*33*, *34*), while this activity is associated with lysozomes and the golgi apparatus in mammalian cells (*35*). These alternatives were evaluated by adding either folate or the folate analogue DMDDF, described in our previous study (*10*), to a sample initially containing 0.5 mM R67 DHFR and 5 mM $NADP^+$. In general, folate will increase the affinity of the enzyme for $NADP^+$, though it can also weaken binding by competing directly for the binding site. Alternatively, we previously found that the folate analogue DMDDF had a much stronger tendency to form ternary $(DMDDF)_2$−DHFR complexes than to form ternary DMDDF−$NADP^+$−DHFR complexes. As shown in Figure 5, addition of 25 mM folate increased the apparent rate of the phosphatase reaction, while addition of 10 mM folate analogue DMDDF decreased the rate of dephosphorylation (as measured by the intensity of the NAD^+ nicotinamide NH-2 peak). Since neither folate nor DMDDF would be expected to affect the rate of $NADP^+$ dephosphorylation because of the presence of contaminating $NADP^+$ phosphatase, these results provide a clear indication that the observed dephosphorylation results from the interaction of $NADP^+$ with the R67 DHFR. Fitting the data in Figure 5 to first-order kinetics gave initial rate constants (turnover numbers) of 1.05×10^{-5} s^{-1} for DHFR and $NADP^+$, 3.05×10^{-5} s^{-1} for DHFR, $NADP^+$, and folate, and 1.73×10^{-6} s^{-1} for DHFR, $NADP^+$, and DMDDF. Hence, the primary effect of folate appears to be an enhancement of the side reaction as a result of cooperative binding of $NADP^+$ by the folate−DHFR complex. The effect of DMDDF is, as previously found, to block the binding of $NADP^+$ and hence the phosphatase reaction.

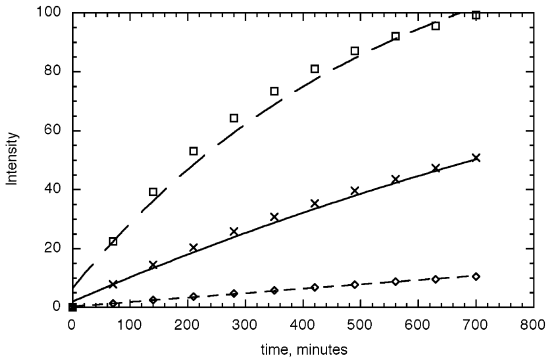

FIGURE 5: Kinetics of $NADP^+$ dephosphorylation, catalyzed by R67 DHFR (0.5 mM), as measured by the intensity of the NAD^+ NH-2 peak: (×) 5 mM $NADP^+$ alone, (□) 5 mM $NADP^+$ and 25 mM folate, and (◇) 5 mM $NADP^+$ and 10 mM DMDDF.

Reduction of $NADP^+$ to NADPH in the Ternary $NADP^+$−NADPH−DHFR Complex. In contrast with chromosomal DHFR, type II DHFR can form ternary complexes involving two pterin molecules or two pyridine nucleotides (*8*). Bradrick et al. reported that titration of the NADPH−DHFR complex with $NADP^+$ was characterized by a dissociation constant of 88 ± 8 μM, indicating the formation of a ternary $NADP^+$−NADPH−DHFR complex (*8*). Proton interligand Overhauser effect (ILOE) studies performed on samples containing 1 mM $NADP^+$ and 1 mM NADPH in the presence of 0.1 mM R67 DHFR revealed significant cross-peaks connecting the N-4A and N-4B resonances of NADPH with the N-4 and N-5 resonances of $NADP^+$ (Figure 6). These

[2] The following experiments were attempted: isotope-filtered CN NOESY of labeled DHFR with unlabeled $NADP^+$ (*30*) and comparison of decoupled and coupled NOESY spectra of labeled DHFR with unlabeled $NADP^+$ (*31*).

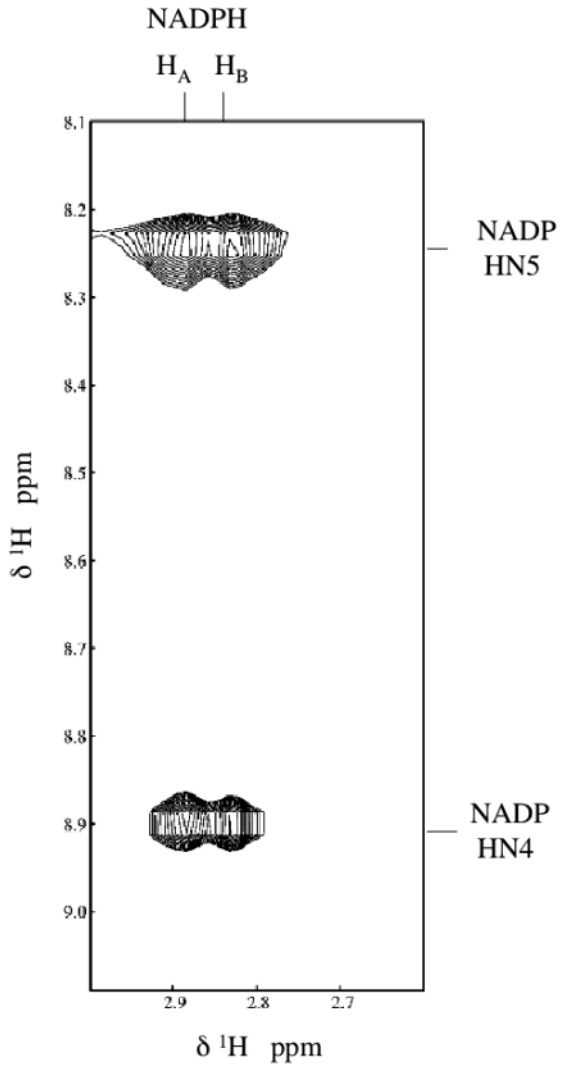

FIGURE 6: Region of an NOE spectrum of 1 mM $NADP^+$, 1 mM NADPH, and 0.1 mM R67 DHFR showing the cross-peaks connecting NADPH H-4_A/H-4_B and $NADP^+$ HN-4 and HN-5 resonances. Cross-peaks are labeled. The NMR samples were prepared in 25 mM phosphate in D_2O, with an uncorrected pH of 7.1, at 25 °C. NMR spectral parameters were as follows: spectral width in F_1 of 6500 Hz and in F_2 of 6500 Hz, 256 complex points for t_1 and 512 for t_2, 64 scans per t_1 increment, mixing time of 300 ms, and recycle delay of 1 s.

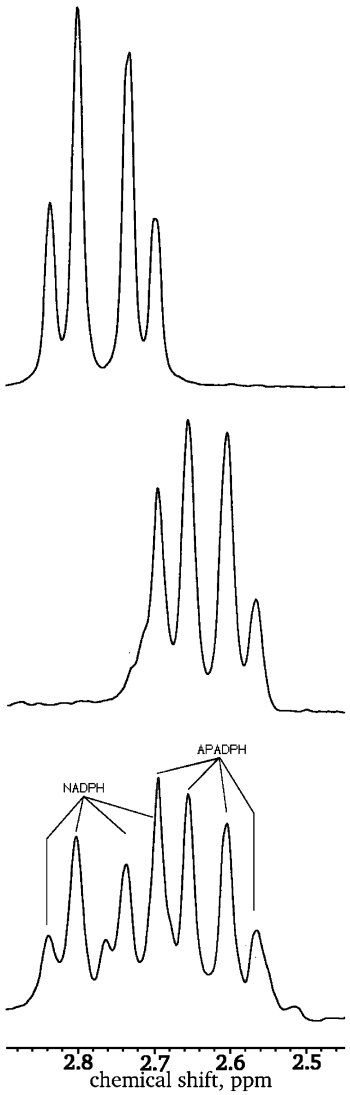

FIGURE 7: (Top) ^{1}H NMR spectrum of 1 mM NADPH. Peaks due to H-4_A (downfield) and H-4_B (upfield) are shown. (Middle) ^{1}H NMR spectrum of APADPH formed by reduction of 1 mM $APADP^+$ by 10 mM $NaCNBH_3$. (Bottom) ^{1}H NMR spectrum of 1 mM $APADP^+$, 1 mM NADPH, and 10 μM DHFR after incubation for 20 h at 25 °C. Peaks due to the presence of APADPH and NADPH are noted.

cross-peaks, which have negative intensity as expected for ILOE interactions in a high-molecular weight system, indicate that a ternary complex is formed with the corresponding protons in close proximity. However, in the case of this ternary complex, there is also the possibility of hydride ion transfer between NADPH and $NADP^+$, which would be consistent with the proximity of the nuclei. Hence, we may be observing a combined NOE and EXSY signal due to both NOE and chemical exchange reactions.

To more fully evaluate the latter, we utilized the $NADP^+$ analogue 3-acetylpyridine adenine dinucleotide phosphate ($APADP^+$). Evidence for hydride transfer from NADPH to $APADP^+$, yielding $NADP^+$ and APADPH, can be seen in Figure 7. This figure illustrates the upfield spectra of NADPH (top trace), APADPH (middle trace, prepared by reduction of $APADP^+$ by sodium cyanoborohydride), and the products of a reaction mixture initially containing $APADP^+$, NADPH, and DHFR (bottom trace). We note that in the latter sample, the presence of both reduced nucleotides is apparent. A residual acetyl methyl resonance arising from the oxidized $APADP^+$ is also present in the middle and bottom spectra, overlapping the farthest downfield resonance of the NADPH or APADPH AB quartet. This reaction (hydride transfer from NADPH to $APADP^+$ catalyzed by DHFR) is more than 50% complete in 20 h (approximate turnover number of 10^{-6} s^{-1}). In contrast, the reaction in the absence of enzyme is slower, approximately 17% complete in the same time period. Thus, the existence of a DHFR-catalyzed hydride transfer is confirmed. Assuming that the DHFR catalyzes an analogous hydride exchange reaction between NADPH and $NADP^+$, the exchange reaction will also contribute to the observed cross-peaks connecting the H-4 resonances of $NADP^+$ and NADPH. However, on the basis of the rates observed using the $NADP^+$ analogue, it appears that this reaction is probably too slow to contribute significantly, suggesting that the observed cross-peaks arise primarily due to an interligand

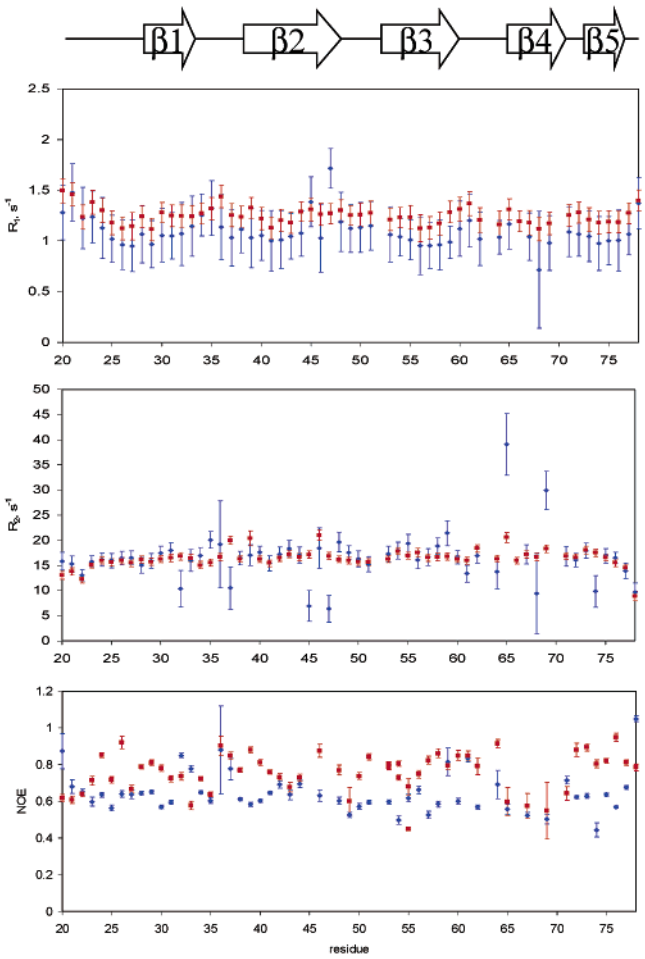

FIGURE 8: Relaxation parameters for R67 DHFR. Shown are (A) R_1, (B) R_2, and (C) NOE values as a function of protein sequence. The data correspond to 1 mM DHFR (red) or to 1 mM DHFR and 1 mM NADP$^+$ (blue). Samples were run in 25 mM phosphate at pH 7.0 and 25 °C. Data were collected at a ^{1}H frequency of 500 MHz for DHFR and 600 MHz for DHFR and NADP$^+$. Error bars are standard errors given by the modified relaxation analysis module of NMRView.

Overhauser effect, rather than as a result of chemical exchange.

Dynamic Characterization. The dynamic behavior of R67 DHFR on a time scale of nanoseconds to picoseconds was assessed by measuring ^{15}N T_1, ^{15}N T_2, and steady state ^{15}N-{^{1}H} NOE relaxation parameters at ^{1}H frequencies of 500 MHz (DHFR alone) and 600 MHz (DHFR and NADP$^+$). The R_1, R_2, and NOE data obtained in the absence and presence of NADP$^+$ are shown in Figure 8. A noticeable feature is the uniformity about the mean of R_1, R_2, and heteronuclear NOE data for free DHFR, indicative of a well-structured protein with relatively little backbone motion. A more detailed analysis of the protein dynamics was obtained using the program Modelfree (*22*). An initial fit of a restricted data set (the trimmed mean of T_1/T_2 data) to models that assumed isotropic, axially symmetric, or fully asymmetric overall molecular tumbling indicated that the axially symmetric model provided an optimal fit using the fewest experimental parameters (*21*). For this model, the $D_{||}/D_{\perp}$ ratio was calculated to be 0.85. This result is consistent with a calculation of the elements of the moments of inertia tensor for the molecule (I_{zz} = 1.0, I_{yy} = 1.2, and I_{xx} = 1.5). The relaxation data were then fit using the Modelfree program

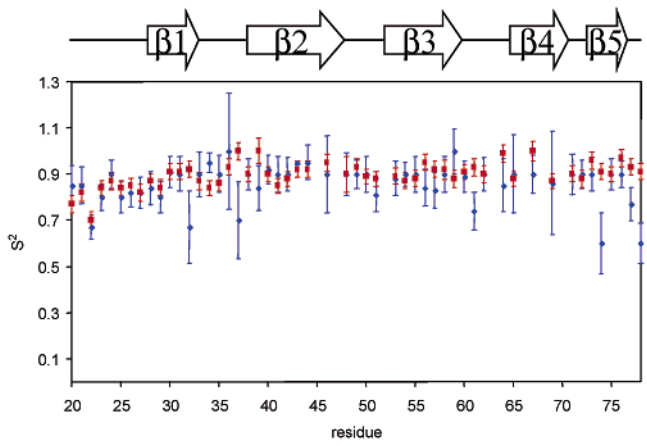

FIGURE 9: Order parameter S^2 for R67 DHFR in the presence (blue) and absence (red) of NADP$^+$, as determined by Modelfree analysis of the data shown in Figure 2. The sample contained 1 mM DHFR (red) or 1 mM DHFR and 1 mM NADP$^+$ (blue). Error bars are standard errors given by Modelfree.

Table 1: Summary of Model Selection[a]

	DHFR only		DHFR and NADP$^+$	
model	no. of residues	%	no. of residues	%
1	32	57.1	10	17.9
2	21	37.5	45	80.3
3	1	1.8	0	0
4	1	1.8	1	1.8
5	1	1.8	0	0

[a] The different motional models for R67 DHFR in the absence and presence of NADP$^+$ are compared. The number and percentage of residues that fit to a given model are given. Sample concentrations were 1 mM DHFR and (when present) 1 mM NADP$^+$. Samples were run in 25 mM phosphate at pH 7.0 and 25 °C. Data were collected at a ^{1}H frequency of 500 MHz for DHFR and 600 MHz for DHFR and NADP$^+$.

(*22*) and Akaike's Information Criteria (AIC) (*23*) was used to identify the most appropriate motional model. Generalized order parameters (S^2) determined using this procedure are shown in Figure 9, which reveals that there is not much difference in the overall motion of DHFR upon binding of NADP$^+$ ($\langle S_{free}^2 \rangle$ = 0.89; $\langle S_{bound}^2 \rangle$ = 0.86). The model selection is summarized in Table 1. As is apparent from this table, there was little need to invoke conformational exchange processes for a majority of the resonances. Only two residues in the DHFR study, and one in the DHFR and NADP$^+$ study, required the use of models with R_{ex} added to R_2. However, the addition of NADP$^+$ to DHFR affected the distribution of models selected by AIC for most residues. As shown in Table 1, the majority (57%) of residues in free DHFR fit best to model 1, while a greater percentage (80%) of residues in DHFR and NADP$^+$ fit best to model 2. This shift in model distribution could indicate additional molecular motion present upon binding of NADP$^+$ (*vide infra*). We note that in the presence of NADP$^+$, the dynamic behavior of each of the four subunits can differ significantly. Since the resonances for each subunit are degenerate on the chemical shift time scale, we are able to observe only a weighted average of the relaxation parameters. In the event that one of the subunits exhibits very different relaxation behavior, the effects may be largely diluted by the contributions from the other three subunits. This is an inherent limitation arising in the analysis

of the relaxation behavior of degenerate systems such as the R67 DHFR.

Once $NADP^+$ binds, the R_2 values for the amide ^{15}N nuclei of Ser65 and Tyr69 increase significantly. Most probably, these increases arise from exchange contributions due to variations in the relative positioning of the $NADP^+$ on a micro- to millisecond time scale. Such exchange is anticipated because of the relatively weak binding of $NADP^+$, and could correspond to kinetic sampling by $NADP^+$ of the four symmetry-related binding sites in the DHFR pore. As discussed in the following section, the large shift and the exchange broadening of the Ser65 amide resonance probably reflect the variability of the Ser65−His62 hydrogen bonding interaction that forms a β-turn. Significant deviations from the mean value of S^2 were observed for residues Lys32, Ala37, Ala61, Leu74, and Asn78. As discussed below, Lys32 is undoubtedly involved in $NADP^+$ binding, so it is not unexpected that the motion of this residue is altered in the presence of $NADP^+$. Leu74, located at the mouth of the central pore, also exhibits a large shift upon binding of $NADP^+$. The motional perturbation of Ala37 and Ala61 may result from a conformational change. Interestingly, the Ala36 resonance is significantly broadened in the HSQC spectrum of the free enzyme. Alanine 36 and alanine 37 are on a loop connecting β-strands 1 and 2 and are also situated at an interchain contact point. Hence, the relative motion of the peptide chains may also be partly responsible for the reduced order parameter.

DISCUSSION

Type II DHFR appears to have evolved to provide a resistance mechanism to bacterial antifolate drugs such as trimethoprim (*3*−*6*). Perhaps the most remarkable feature of type II DHFR is the lack of separately defined substrate and cofactor binding sites. Nevertheless, the enzyme retains the ability to catalyze a stereospecific hydride transfer reaction. The goal of this study has been to understand the nature of the interaction of $NADP^+$ with this enzyme. The NMR data obtained for the labeled DHFR indicate that all four peptide chains are magnetically equivalent, consistent with the symmetry observed in the crystalline state. The observation of an elevated *cis*:*trans* ratio for the Phe18−Pro19 bond indicates that both imide bond conformations can be accommodated in the folded structure. Recently, Bodenreider et al. (*28*) have studied the folding of R67 DHFR and observed a slow phase that was attributed to peptidyl−proline bond isomerization. Since the folded structure can accommodate both isomers of the Phe18−Pro19 pair, the conformation of this particular Phe−Pro bond is probably not rate-limiting in the folding process.

The observed magnetic equivalence of the four peptide chains was preserved upon addition of the cofactor product, $NADP^+$. Since binding of $NADP^+$ would be expected to lift the shift degeneracy of the resonances for the four chains, this result is consistent with weak binding, which results in averaging of the chemical shift perturbations on a time scale faster than the chemical shift time scale. Shift titrations of the amide resonances most sensitive to $NADP^+$ binding yielded a mean dissociation constant K_D of 133 μM, similar to the value of 99 μM obtained from ITC studies (*8*). In general, the largest amide shifts were observed for residues located in the pore on strand β4. These residues are expected to be in direct contact with the $NADP^+$ (*7*, *29*). Significant shifts were also observed for Lys32 as well as the amide groups of nearby residues, consistent with the interaction of Lys32 with the phosphate groups of $NADP^+$. Larger shifts for some of the other amide groups, such as Ala73, Leu74, Trp45, and Tyr46, are less readily interpreted. Since all of these residues are positioned in the β-sheet of the molecule, it is possible that binding produces structural perturbations that are transmitted throughout the β-sheet. Thus, local changes in hydrogen bonding interactions, rather than proximity to the $NADP^+$, may be the primary factor responsible for these shifts. A similar effect is observed for the amide of Ser65, which is involved in a hydrogen bond to His62 as part of a β-turn. As shown in Figure 3, this amide group exhibits the largest shift in response to $NADP^+$ binding. Nevertheless, kinetic analysis of the S65A mutant R67 DHFR indicates that this residue is apparently not required for NADPH binding (*36*). As in the example above, a perturbation of the β-sheet structure coincident with $NADP^+$ binding is probably responsible for most of the Ser65 amide shift perturbation. This interpretation highlights a potentially interesting aspect of the use of amide shifts to monitor binding interactions. Nevertheless, interpretation of chemical shift data for the type II DHFR is subject to the unique constraints that result from the symmetry of the molecule. It is quite possible in this case to have a large shift for a residue in chain A, for example, balanced by small negative shifts for the corresponding residue in chains B−D, resulting in a null observation.

Although there are insufficient data to develop a detailed model for the binding of $NADP^+$ to DHFR, the data obtained here in combination with previous studies (*7*−*10*, *12*, *36*) support a model in which the nicotinamide base of $NADP^+$ binds at the center of the pore, resulting in large shifts for an amide side chain which we have identified as Q67. The conformation of the $NADP^+$ is approximately extended, with the diphosphodiester interacting with one of the Lys32 residues and with a Tyr69 residue. The former provides a favorable electrostatic interaction, while the latter has been identified as being important for $NADP^+$ binding in modeling (*29*) and mutagenesis (*36*) studies. The adenine base is positioned near the mouth of the pore, and the adenosyl 2′-phosphate extends back into the pore where it interacts with a second Lys32 residue. Such an interaction is important for explaining the strong preference of the enzyme for NADPH relative to NADH (*37*). Examination of the structures of a broad range of NADP(H)-dependent enzymes in the Protein Data Bank indicates that the interaction with the cofactor is mediated by two cationic residues (lysine and/or arginine) that interact with the diphosphodiester and with the adenosyl 2′-phosphate. Studies of the effects of NaCl on enzyme kinetic behavior reveal that the K33M mutant behaves in a manner essentially identical to that of the wild-type enzyme (S. N. Hicks et al., *Biochemistry*, in press), indicating that any favorable electrostatic contributions to dinucleotide binding are derived from Lys32. Further, positioning of the adenosyl 2′-phosphate in the core is probably required to explain the observed phosphatase activity. Modeling studies have suggested that the adenine may be positioned near Ala36, Gly64, and Thr51. The Gly64 amide exhibits a strong

shift sensitivity to $NADP^+$ binding, while the shifts for Ala36 and Thr51 are closer to the mean values.

Proton NMR studies of a mixture of NADPH and $NADP^+$ performed in the presence of DHFR also demonstrate that in the ternary NADPH−$NADP^+$−DHFR complex, the proximity of the NADPH H-4 protons to the $NADP^+$ H-4 and H-5 protons is sufficient to produce observable cross-peaks. These resonances can arise due to interligand Overhauser effects between the corresponding protons, as observed previously, for example, in ternary $NADP^+$−folate−DHFR complexes (*10*). Alternatively, it is also possible that these are "EXSY" peaks that result from direct transfer of a hydride ion from the NADPH to $NADP^+$. In general, if the H-4 protons of the two molecules are sufficiently close to produce observable NOE cross-peaks, it would not be surprising for hydride transfer to occur so that the observed cross-peaks could arise from both effects. To determine whether the enzyme can, indeed, catalyze an NADPH−$NADP^+$ hydride transfer reaction, we replaced the $NADP^+$ with its acetyl pyridine analogue, $APADP^+$. The latter compound contains an acetyl group instead of the amide group of $NADP^+$. Smith and Burchall (*37*) have demonstrated that the reduced form of this analogue, APADPH, can function as a cofactor in dihydrofolate reduction by R67 DHFR, as well as DHFR from several other sources. As demonstrated here, we found that in the presence of NADPH, $APADP^+$ is gradually reduced. The process is accelerated in the presence of R67 DHFR, but still requires many hours to reach equilibrium. Hence, the observed proton cross-peaks in the sample containing $NADP^+$, NADPH, and DHFR probably arise predominantly from an interligand Overhauser effect, rather than from a hydride transfer reaction.

The observed dephosphorylation of $NADP^+$ to produce NAD^+ was an unanticipated result of this study. The ability of folate and a folate analogue to modulate the dephosphorylation rate provides strong support for the conclusion that this reaction is being catalyzed by DHFR rather than by a contaminating phosphatase. Although the mechanism for such a reaction is unknown, we propose the following possibility. The strong preference of R67 DHFR for NADPH over NADH indicates a specific interaction with the adenosyl 2′-phosphate group, presumably arising from an interaction with K32 located in the pore of the enzyme. The location of this residue in the hydrophobic pore enhances the likelihood of a deprotonated NH_2 form, which can act as a nucleophile. The lysyl NH_2 group might act by deprotonating a water molecule to produce a hydroxyl ion. The presence of the bound $NADP^+$ phosphate group and a hydroxyl ion positioned near K32 could then result in a hydrolytic reaction as the hydroxyl group attacks the adenosyl phosphorus nucleus. This model for catalytic activity is analogous to the hydrolysis reactions catalyzed by many nucleases. Although a more complex reaction involving the formation of a phosphorylated enzyme intermediate is also possible, it would be necessary to hydrolyze the phosphate group in a subsequent step. This more complex alternative seems to be less likely to characterize a side reaction such as the $NADP^+$ dephosphorylation described here.

Brito et al. (*12*) have previously performed NMR studies on a binary complex of a related type II DHFR on the R388 plasmid and $NADP^+$. They observed time-dependent changes in the proton spectra of both $NADP^+$ and the DHFR, which were proposed to result from a slow conformational change of the enzyme. For a system containing 5 mM $NADP^+$ and 0.5 mM DHFR studied at 25 °C, this process occurred over a period of hours (*12*). Under the conditions of their study, the conformational change appeared to be irreversible. For the initial system, with the enzyme in "conformation I", the nicotinamide NH-2 and NH-6 resonances of $NADP^+$ were broad and shifted significantly upfield. For the system in "conformation II", the NH-2 and NH-6 resonances of the $NADP^+$ were considerably sharper and shifted downfield. The reported shift changes are very similar to those that we observed when comparing the NH-2 and NH-6 resonances of NAD^+ to those of $NADP^+$. The somewhat larger shifts (0.055 ppm) observed in this work result from the higher pH of our studies. The pH used in the studies presented in this report was 7.0 compared with a pH of 5.9 in the study of Brito et al. (*12*), which results in a more highly charged phosphate group. Thus, the shift differences between NAD^+ and $NADP^+$ increase upon deprotonation of the 2′-phosphate of the AMP moiety. Therefore, the observation of two sets of resonances for NH-2 and NH-6 protons in the prior study is completely consistent with the interpretation that these correspond to a mixture of $NADP^+$ and NAD^+, rather than to two enzyme conformations. The apparent decreased line widths of the NH-2 and NH-6 resonances for R388 DHFR in conformation II observed by Brito et al. are also consistent with this conclusion, since the binding of NAD^+ to DHFR is much weaker, so that the exchange will be much faster, reducing the magnitude of the exchange broadening effect.

Brito et al. (*12*) also observed time-dependent changes in the ^1H NMR spectra of the upfield-shifted methyl resonances of the R388 DHFR (Figure 8 of ref *12*). Qualitatively, the spectra were significantly perturbed immediately after the addition of the $NADP^+$, followed by a slow reversion back toward a spectrum that more closely resembled the spectrum before addition of the $NADP^+$. The latter changes occurred on the same time scale as the changes in the $NADP^+$ spectrum. These time-dependent changes are also consistent with an $NADP^+ \rightarrow NAD^+$ reaction, since the latter will bind much more poorly with the enzyme, resulting in a spectrum that is more similar to that of the apoenzyme. In summary, we believe that the $NADP^+$ phosphatase activity of the type II DHFR molecules is a general phenomenon, and provides an attractive alternative explanation for the spectral changes observed in the previous study of R388 DHFR (*12*).

The dynamics and chemical shift titration studies presented here have identified a few key residues that exhibit changes upon binding of $NADP^+$. Furthermore, the observed lack of large-scale global changes in backbone dynamics is consistent with the view that the backbone structure of R67 DHFR is designed to provide a stable surface or pore where the reaction can be catalyzed. This is in stark contrast to type I DHFR, where the motions of backbone atoms of different loops are proposed to be critical to function (*38*−*40*).

ACKNOWLEDGMENT

We express our appreciation to Dr. Guihua Yue of the National Institute of Environmental and Health Sciences Mass Spectrometry group for providing mass spectrometric data on the NADP breakdown products and to Dr. David Houck for helpful discussions.

REFERENCES

1. Hitchings, G. H., and Burchall, J. J. (1965) Inhibition of folate biosynthesis as a basis for chemotherapy, *Adv. Enzymol. Relat. Areas Mol. Biol. 27*, 417−468.
2. Burchall, J. J., and Hitchings, G. H. (1965) Inhibitor binding analysis of dihydrofolate reductases from various species, *Mol. Pharmacol. 1*, 126−136.
3. Fleming, M. P., Datta, N., and Gruneberg, R. N. (1972) Trimethoprim resistance determined by R factors, *Br. Med. J. 1*, 726−728.
4. Pattishall, K. H., Acar, J., Burchall, J. J., Goldstein, F. W., and Harvey, R. J. (1977) Two Distinct Types of Trimethoprim-resistant Dihydrofolate Reductase Specified by R-Plasmids of Different Compatibility Groups, *J. Biol. Chem. 252*, 2319−2323.
5. Smith, S. L., Stone, D., Novak, P., Baccanari, D. P., and Burchall, J. J. (1979) R Plasmid Dihydrofolate Reductase with Subunit Structure, *J. Biol. Chem. 254*, 6222−6225.
6. Stone, D., and Smith, S. L. (1979) The Amino Acid Sequence of the Trimethoprim-resistant Dihydrofolate Reductase Specified in *Escherichia coli* by R-Plasmid R67, *J. Biol. Chem. 254*, 10857−10861.
7. Narayana, N., Matthews, D. A., Howell, E. E., and Xuong, N. (1995) A plasmid-encoded dihydrofolate reductase from trimethoprim-resistant bacteria has a novel D_2-symmetric active site, *Nat. Struct. Biol. 2*, 1018−1025.
8. Bradrick, T. D., Beechem, J. M., and Howell, E. E. (1996) Unusual binding stoichiometries and cooperativity are observed during binary and ternary complex formation in the single active pore of R67 Dihydrofolate Reductase, a D_2 symmetric protein, *Biochemistry 35*, 11414−11424.
9. Brito, R. M. M., Rudolph, F. B., and Rosevear, P. R. (1991) Conformation of $NADP^+$ Bound to a Type II Dihydrofolate Reductase, *Biochemistry 30*, 1461−1469.
10. Li, D., Levy, L. A., Gabel, S. A., Lebetkin, M. S., DeRose, E. F., Wall, M. J., Howell, E. E., and London, R. E. (2001) Interligand Overhauser Effects in Type II Dihydrofolate Reductase, *Biochemistry 40*, 4242−4252.
11. Gourley, D. G., Schüttelkopf, A. W., Leonard, G. A., Luba, J., Hardy, L. W., Beverley, S. M., William, N., and Hunter, W. N. (2001) Pteridine reductase mechanism correlates pterin metabolism with drug resistance in trypanosomatid parasites, *Nat. Struct. Biol. 8*, 521−525.
12. Brito, R. M. M., Reddick, R., Bennett, G. N., Rudolph, F. B., and Rosevear, P. R. (1990) Characterization and Stereochemistry of Cofactor Oxidation by a Type II Dihydrofolate Reductase, *Biochemistry 29*, 9825−9831.
13. Reece, L. J., Nichols, R., Ogden, R. C., and Howell, E. E. (1991) Construction of a synthetic gene for an R-plasmid-encoded dihydrofolate reductase and studies on the role of the N-terminus in the protein, *Biochemistry 30*, 10895−10904.
14. Muhandiram, D. R., and Kay, L. E. (1994) Gradient-Enhanced Triple-Resonance Three-Dimensional NMR Experiments with Improved Sensitivity, *J. Magn. Reson., Ser. B 103*, 203−216.
15. Grzesiek, S., Anglister, J., and Bax, A. (1993) Correlation of Backbone Amide and Aliphatic Side-Chain Resonances in $^{13}C/^{15}N$-Enriched Proteins by Isotropic Mixing of ^{13}C Magnetization, *J. Magn. Reson., Ser. B 101*, 114−119.
16. Logan, T. M., Olejniczak, E. T., Xu, R. X., and Fesik, S. W. (1993) A general method for assigning NMR spectra of denatured proteins using 3D HC(CO)NH-TOCSY triple resonance experiments, *J. Biomol. NMR 3*, 225−231.
17. Farrow, N. A., Muhandiram, R., Singer, A. U., Pascal, S. M., Kay, C. M., Gish, G., Shoelson, S. E., Pawson, T., Forman-Kay, J. D., and Kay, L. E. (1994) Backbone dynamics of a free and a phosphopeptide-complexed SRC Homology-2 domain studied by N-15 NMR relaxation, *Biochemistry 33*, 5984−6003.
18. Delaglio, F., Grzesiek, S., Vuister, G. W., Zhu, G., Pfeifer, J., and Bax, A. (1995) NMRPipe: a multidimensional spectral processing system based on UNIX pipes, *J. Biomol. NMR 6*, 277−293.
19. Johnson, B. A., and Blevins, R. A. (1994) NMR View: a computer-program for the visualization and analysis of NMR data, *J. Biomol. NMR 4*, 603−614.
20. Pari, K., Mueller, G. A., DeRose, E. F., Kirby, T. W., and London, R. E. (2003) Solution Structure of the RNase H Domain of the HIV-1 Reverse Transcriptase in the Presence of Magnesium, *Biochemistry 42*, 639−650.
21. Kroenke, C. D., Loria, J. P., Lee, L. K., Rance, M., and Palmer, A. G. (1998) Longitudinal and Transverse ^1H-^{15}N Dipolar/^{15}N Chemical Shift Anisotropy Relaxation Interference: Unambiguous Determination of Rotational Diffusion Tensors and Chemical Exchange Effects in Biological Macromolecules, *J. Am. Chem. Soc. 120*, 7905−7915.
22. Tjandra, N., Feller, S. E., Pastor, R. W., and Bax, A. (1995) Rotational Diffusion Anisotropy of Human Ubiquitin from N-15 NMR Relaxation, *J. Am. Chem. Soc. 117*, 12562−12566.
23. Mandel, A. M., Akke, M., and Palmer, A. G., III (1995) Backbone Dynamics of *Escherichia coli* Ribonuclease HI: Correlations with Structure and Function in an Active Enzyme, *J. Mol. Biol. 246*, 144−163.
24. d'Auvergne, E. J., and Gooley, P. R. (2003). The use of model selection in the model-free analysis of protein dynamics, *J. Biomol. NMR 25*, 25−39.
25. Wishart, D. S., and Sykes, B. D. (1994) The C-13 Chemical-Shift Index: a simple method for the identification of protein secondary structure using C-13 chemical-shift data, *J. Biomol. NMR 4*, 171−180.
26. Bedford, G. R., and Sadler, P. J. (1974) ^{13}C magnetic resonance study of the ionization of *N*-acetyl-DL-proline in aqueous solution, *Biochim. Biophys. Acta 343*, 656−662.
27. Wu, W. J., and Raleigh, D. P. (1998) Local Control of Peptide Conformation: Stabilization of *cis* Proline Peptide Bonds by Aromatic Proline Interactions, *Biopolymers 45*, 381−394.
28. Bodenreider, C., Kellershohn, N., Goldberg, M. E., and Mejean, A. (2002) Kinetic Analysis of R67 Dihydrofolate Reductase Folding: From the Unfolded Monomer to the Native Tetramer, *Biochemistry 41*, 14988−14999.
29. Howell, E. E., Shukla, U., Hicks, S. N., Smiley, R. D., Kuhn, L. A., and Zavodsky, M. I. (2001) One site fits both: a model for the ternary complex of folate + NADPH in R67 dihydrofolate reductase, a D2 symmetric enzyme, *J. Comput.-Aided Mol. Des. 15*, 1035−1052.
30. Zwahlen, C., Legault, P., Vincent, S. J. F., Greenblatt, J., Konrat, R., and Kay, L. E. (1997) Methods for Measurement of Intermolecular NOEs by Multinuclear NMR Spectroscopy: Application to a Bacteriophage λ N-Peptide/boxB RNA Complex, *J. Am. Chem. Soc. 119*, 6711−6721.
31. Boetzel, R., Czisch, M., Kaptein, R., Hemmings, A. M., James, R., Kleanthous, C., and Moore, G. R. (2000) NMR investigation of the interaction of the inhibitor protein Im9 with its partner DNase, *Protein Sci. 9*, 1709−1718.
32. Andres, J., Moliner, V., Safont, V. S., Domingo, L. R., Picher, M. T., and Krechl, J. (1996) On transition structures for hydride transfer step: A theoretical study of the reaction catalyzed by dihydrofolate reductase enzyme, *Bioorg. Chem. 24*, 10−18.
33. Richter, C. (1987) $NADP^+$ Phosphatase: A Novel Mitochondrial Enzyme, *Biochem. Biophys. Res. Commun. 146*, 253−257.
34. Gallais, S., de Crescenzo, M. A. P., and Laval-Martin, D. L. (2000) Evidence of active NADP(+) phosphatase in dormant seeds of *Avena sativa* L., *J. Exp. Bot. 51*, 1389−1394.
35. Smith, C. E., Hermo, L., Fazel, A., Lalli, M. F., and Bergeron, J. J. M. (1990), Ultrastructural Distribution of NADPase Within the Golgi-Apparatus and Lysosomes of Mammalian-Cells, *Prog. Histochem. Cytochem. 21*, 1−124.
36. Strader, M. B., Smiley, R. D., Stinnett, L. G., VerBerkmoes, N. C., and Howell, E. E. (2001) Role of S65, Q67, I68, and Y69 residues in homotetrameric R67 dihydrofolate reductase, *Biochemistry 40*, 11344−11352.
37. Smith, S. L., and Burchall, J. J. (1983) α-Pyridine nucleotides as substrates for a plasmid-specified dihydrofolate reductase, *Proc. Natl. Acad. Sci. U.S.A. 80*, 4619−4623.
38. Osborne, M. J., Schnell, J., Benkovic, S. J., Dyson, H. J., and Wright, P. E. (2001) Backbone Dynamics in Dihydrofolate Reductase Complexes: Role of Loop Flexibility in the Catalytic Mechanism, *Biochemistry 40*, 9846−9859.
39. Rajagopalan, P. T. R., Lutz, S., and Benkovic, S. J. (2002) Coupling Interactions of Distal Residues Enhance Dihydrofolate Reductase Catalysis: Mutational Effects on Hydride Transfer Rates, *Biochemistry 41*, 12618−12628.
40. Agarwal, P. K., Billeter, S. R., Rajagopalan, P. T. R., Benkovic, S. J., and Hammes-Schiffer, S. (2002) Network of coupled

promoting motions in enzyme catalysis, *Proc. Natl. Acad. Sci. U.S.A. 99*, 2794−2799.
41. Liang, J., Edelbrunner, H., and Woodward, C. (1998) Anatomy of Protein Pockets and Cavities: Measurement of Binding Site Geometry and Implications for Ligand Design, *Protein Sci. 7*, 1884−1897.

BI0349874